

Bio-high density polyethylene films embedded with organoclay and zinc pyrithione

Priscylla Jordânia Pereira de Mesquita¹ , Cristiano José de Farias Braz¹ , Tatianny Soares Alves¹ 
and Renata Barbosa^{1*} 

¹Laboratório de Polímeros e Materiais Conjugados – LAPCON, Centro de Tecnologia,
Universidade Federal do Piauí – UFPI, Teresina, PI, Brasil

*rrenatabarbosa@yahoo.com

Abstract

Bio-high density polyethylene (BHDPE) films with organoclay and antimicrobial additives (zinc pyrithione) were evaluated. The composites were prepared in a single-screw extruder using the melt intercalation technique, and the films were obtained by flat extrusion. The diffractograms indicated the formation of an intercalated nanocomposite (BHDPE/6 wt% of clay). Infrared spectra suggested that the polymer predominates over the antimicrobial agent bands. Thermal stability was slightly reduced by up to 3°C. The clay and antimicrobial agent reduced the melting point and crystallinity of BHDPE by up to 12 °C and 13.3%, respectively. In addition, the presence of clay and antimicrobial agent significantly ($p < 0.05$) affected all mechanical properties. Proliferation of *Staphylococcus aureus* demonstrated that both evaluated additives did not significantly ($p > 0.05$) inhibit microbial growth. The results emphasize a promising application of the films for packaging that does not require antimicrobial control, with films highlighted by 6 wt% of clay.

Keywords: *cloisite 20a[®], flat films, microbial activity.*

How to cite: Mesquita, P. J. P., Braz, C. J. F., Alves, T. S., & Barbosa, R. (2024). Bio-high density polyethylene films embedded with organoclay and zinc pyrithione. *Polímeros: Ciência e Tecnologia*, 34(1), e20240010. <https://doi.org/10.1590/0104-1428.20230100>

1. Introduction

The change in habits and the increase in consumerism in recent decades led to technological innovations and, consequently, to the greater production of consumer goods, which led to an increase in the production of packaging^[1]. Current packages have specific functions and information to improve quality and food safety. They must increase shelf life and monitor the safety and quality of packaging products. Nanotechnology can extend the essential functions of packaging: containment, protection and preservation, and marketing^[2].

Among the innovations in the plastic packaging, those produced from green polyethylene or biopolyethylene (BPE)^[2,3]. This material has less environmental impact during its synthesis, processing, or degradation than conventional polymers^[3]. It has the same functions, characteristics, and applications as polyethylene (PE) derived from fossil resources. However, BPE uses 70% less fossil fuels and emits approximately 170% less greenhouse gases than PE derived from petroleum. In this way, it becomes a viable alternative to conventional polymers for packaging high-consumption products, such as food packaging^[4].

In this scenario, plastic packaging transformed to become more attractive. It now has known features like active packaging. These active packages have a system that predicts or estimates food quality and safety^[5]. It also releases substances that prolong the shelf life of the product.

Among these innovations, antimicrobial packaging stands out for offering additional protection against microorganisms^[6].

Generally, antimicrobial additives are divided into organic and inorganic systems. Organic materials include phenols, halogenated compounds^[7], and quaternary ammonium salts^[8]. Inorganic materials include metals^[9], phosphates^[10], oxides^[11], and organoclays^[12,13].

Metal complexes, including palladium^[14], copper, nickel^[15], silver, cadmium^[15], present an alternative for incorporation antimicrobial agents. Zinc pyrithione (ZPT), a zinc complex, appears as an option because it is often used in personal care products, such as shampoos and soaps, due to its antifungal and antibacterial properties^[16]. The ZPT has a melting point of 240 °C, which allows for easy processing with most thermoplastics and elastomers, demonstrating compatibility with PE when dispersed in an ethylene vinyl acetate (EVA) matrix^[6].

It is pertinent to highlight that the European Cosmetics Regulation^[17] classifies zinc pyrithione as having reproductive toxicity, making it banned in EU cosmetics since March 2022. On the other hand, the US Food and Drug Administration (FDA)^[18] indicates ZPT as an antimicrobial agent to inhibit bacterial growth on the surface of films made of polyolefin and polyester.

Many studies have evaluated the antimicrobial action of low-density polyethylene (LDPE) films with ZnO^[9,19].

Galli et al.^[6] studied the effect of ZnO in the LDPE/EVA blend, and Rokbani et al.^[20] analyzed the effect of ZnO on LDPE compatibilized with maleic anhydride. Conversely, there are also studies examining the utilization of organoclay, such as Cloisite 15A, 20A, or 30B, as an antimicrobial agent incorporated into PE^[21], LDPE^[22], and linear low-density polyethylene (LLDPE)^[23]. These inquiries indicate that Cloisite 20A clay emerges as a promising alternative for imparting antimicrobial attributes to polymeric films.

Therefore, this study aimed to evaluate and compare the microbial activity of bio-high density polyethylene (BHDPE) films incorporated with organoclay (Cloisite 20A®)^[21-23] and zinc pyrithione dispersed in EVA^[6]. The films were produced by flat extrusion using the melt intercalation technique and characterized by X-ray diffraction (XRD), Fourier transform infrared spectroscopy (FTIR), thermogravimetry (TGA), differential scanning calorimetry (DSC), and tensile test. The antimicrobial activity was assessed against *Staphylococcus aureus*.

2. Materials and Methods

2.1 Materials

Bio-high-density polyethylene (BHDPE), grade SGM9450F, contains at least 96% bio-based (ASTM D6866), melt flow rate of 0.33 g/10min (190 °C/5.0kg -ASTM D1238), was used as received and supplied by BRASKEM (Camaçari, Brazil). The filler incorporated into the BHDPE matrix was Cloisite 20A®, provided by Southern Clay Products (Gonzales, Texas, USA). A commercial antimicrobial agent, marterbach zinc pyrithione dispersed in EVA, Sanitized® MB E 22-70 (Burgdorf, Switzerland), was used as received^[24].

Strains of *Staphylococcus aureus* (ATCC 25923 - Gram-positive) were cultured as target microorganism to evaluate antimicrobial activity. Brain Heart Infusion Broth (BHI) broth agar was used as a culture medium.

2.2 Preparation of nanocomposite films

Samples of BHDPE/Cloisite 20A® and BHDPE/Sanitized® MB E 22-70 (Table 1) were extruded in a single screw extruder AX Plásticos AX-16 (Diadema, Brazil), operating with temperature zones (200, 205, and 210 °C) and screw speed at 50 rpm, as previously reported^[25]. The films were prepared in the same single-screw extruder with the same temperature profile and screw speed of 60 rpm using a flat die of 220 mm width and cylindrical cooling rollers. The formulation of the samples are in Table 1.

2.3 Characterization of films

2.3.1 X-ray diffraction

The crystalline parameters of the films and organoclay were determined using a Shimadzu XRD 6000 (Kyoto, Japan) diffractometer operating in the angular range (2θ) from 5 to 50° using CuKα radiation (λ = 1.5418 Å).

2.3.2 Fourier transform infrared spectroscopy

Changes in the FTIR characteristic band evaluated the interaction between BHDPE, organoclay, and antimicrobial agent. Fourier transform infrared spectroscopy (FTIR) analyses were performed on a Perkin Elmer SPECTRUM 400 (FT-IR/FT-NIR) (Waltham, Massachusetts, USA) spectrometer scanning from 650 to 4000 cm⁻¹ with resolution of 4 cm⁻¹.

2.3.3 Thermal analysis

The thermal stability of the samples was analyzed by thermogravimetry (TGA/DTG) and the thermal behavior and crystallinity of the films were analyzed by differential scanning calorimetry (DSC) using a TA Instrument SDT Q600 V20.9 Build 20 (New Castle, Delaware, USA) equipment, operating at a heating rate of 10 °C.min⁻¹, from room temperature to 550 °C, under argon gas flow (100 mL.min⁻¹). The degree of crystallinity (X_c) of the samples was calculated by Equation 1^[26]:

$$X_c = \left\{ \Delta H_m / \left[(1-w) \Delta H_m^0 \right] \right\} \times 100\% \quad (1)$$

where ΔH_m is the measured heat of fusion, ΔH_m⁰ is the heat of fusion of 100% crystalline HDPE (293 J.g⁻¹)^[27], and w is the weight fraction of organoclay or antimicrobial agent in the polymer matrix. These thermal analyses provide crucial insights into the behaviors of materials in films, which are fundamental for evaluating their suitability in specific applications^[28].

2.3.4 Tensile test

The mechanical behavior of the properties (elastic modulus, strength, and elongation at break) were evaluated according to ASTM D882-18^[29] in a Shimadzu AGS-X universal testing machine with a speed of 20 mm.min⁻¹ and a load cell of 5 kN. Five test specimens were analyzed for each composition in dimensions 120 x 25 mm². Properties were reported in terms of mean ± standard deviation. Tukey's test for post hoc comparisons evaluated the effect of compositions on each property, considering a significance level of 5% (p < 0.05).

Table 1. Formulation of the samples.

Sample	BHDPE	Cloisite 20A®	Sanitized® MB E 22-70
BHDPE	100.0	-	-
PC3	97.0	3.0	-
PC6	94.0	6.0	-
PB1	99.5	-	0.5
PB2	99.0	-	1.0

Formulations expressed in wt% in relation to the polymeric matrix.

2.3.5 Antimicrobial activity

Staphylococcus aureus (ATCC 25923 - Gram-positive) was used as the target microorganism to evaluate antimicrobial activity^[12,13]. The strain was first cultured in brain heart infusion (BHI) agar and placed in an incubator BOD Lucadema Luca 161/01 (São José do Rio Preto, Brazil) at 37 °C for 24 h. Subsequently, films incorporated with the antimicrobial agent were submerged in a suspension containing approximately 10^6 CFU.mL⁻¹ of bacteria were used to contaminate the samples and 10 ml of BHI broth^[30]. As a positive control, test tubes containing only BHI broth and bacterial suspension, and as a negative control, test tubes with BHI broth and BHDPE were used. All test tubes were incubated at 37°C for 4 h. Then, serial dilutions were performed, seeded in Petri dishes containing standard agar for counting and incubated at 37°C for 48 h. The test was performed in triplicate, and the results were expressed in colony-forming units per milliliter (CFU.mL⁻¹). Antimicrobial activity was evaluated based on antimicrobial performance and sensitivity standards^[30,31]. The effect of different compositions on antimicrobial activity was statistically evaluated by Tukey's test for post hoc comparisons, considering a significant difference of 5%.

3. Results and Discussions

3.1 Structural characterization

XRD diffraction patterns of organoclay (Cloisite 20A®), pure BHDPE, and their films containing clay (PC3 and PC6) and antimicrobial additive (PB1 and PB2) are in Figure 1.

Three crystalline peaks on BHDPE can be verified (Figure 1-a), the most intense in the angular range at $2\theta = 21.5^\circ$ corresponding to the (110) plane, the other two less intense at $2\theta = 23.9^\circ$ and $2\theta = 36.4^\circ$ corresponding to the (200) and (020) plans, respectively. These data corroborate the semicrystalline of BHDPE^[25], and the peaks match the specific crystallographic planes. Cloisite 20A® has characteristic peak at $2\theta = 3.40^\circ$ corresponding to (001) plane associated with the galleries that are expanded by the presence of organic salt, as well as the peaks at 2θ equal to 7.06° corresponding to the (002) plane, corroborating the data reported in the literature^[32].

The diffraction planes (position 2θ) were slightly shifted to smaller angles with basal distance $d_{001} = 2.64$ nm in organophilic clay to 2.63 nm and 2.97 nm in systems PC3 and PC6, respectively (Figure 1-b). This displacement suggests that there was even a partial interlacing of the polymeric chains between the clay layers. The formation of a possible intercalated/exfoliated nanocomposite in PC6 film, as previously reported^[33]. Dias et al.^[33] systematically examined the structural attributes of polyurethane nanocomposites containing inorganic particles, specifically synthetic talc and organophilic clay. At the same time, the plans incorporating the antimicrobial additive did not change the structure of the polymeric matrix. Similar results were found in different nanocomposites HDPE/chlorhexidine diacetate^[34].

3.2 Infrared spectroscopy (FTIR)

Infrared spectra in the region of 500 to 4000 cm⁻¹ of pure BHDPE, Cloisite 20A® clay, antimicrobial agent, and their films containing clay (PC3 and PC6) and antimicrobial additive (PB1 and PB2) are in Figure 2.

BHDPE infrared spectrum presents transmission bands close to 2900 and 1450 cm⁻¹, which correspond to the axial and angular deformation movements of the C–H bonds, respectively, and close to 1380 cm⁻¹, which corresponds to the symmetric angular deformation of the methyl group^[35]. The band at 720 cm⁻¹ refers to the C–H vibration of the –CH₂– groups of the amorphous part^[36].

Cloisite 20A® clay spectrum has a considerable absorption at 1023cm⁻¹ attributed to the extension of the Si–O band^[37]. Characteristic bands of BHDPE were maintained in the PB1 and PB2 systems and possibly overlapped those of the antimicrobial additive due to the low content. It detected a small band close to 1000 cm⁻¹ in PC3 and PC6 films, referring to the Si–O bond^[38].

The bands at 3636 and 3395 cm⁻¹ are attributed to O–H stretching from silicate and water, respectively. At 1639 cm⁻¹ is related to O–H bending, and 1040 cm⁻¹ is due to Si–O–Si stretching vibration from silicate^[39]. According to Cervantes-Uc et al.^[39], some bands in organoclay samples spectra which cannot exhibited in the sodium clays.

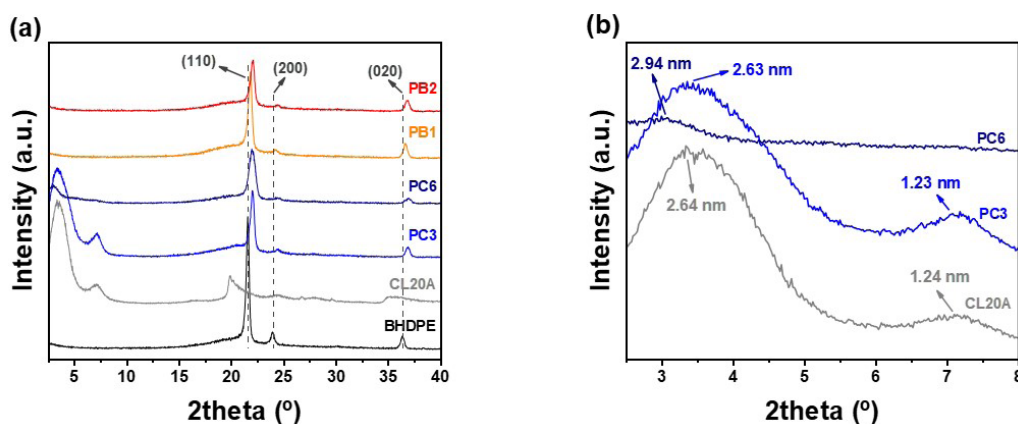


Figure 1. (a) X-ray diffraction patterns of BHDPE, clay, PC3, PC6, PB1 and PB2 systems, and (b) detail of the displacement of the characteristic clay peaks in the PC3 and PC6 systems.

These bands were attributed to C–H vibrations of asymmetric stretching, symmetric stretching and bending of the methylene groups located at 2924, 2842 and 1475 cm^{-1} , respectively, in the chemical structure of the surfactant.

According to Zhang et al.^[40], the powerful absorption at 1050 cm^{-1} may be assigned to the Si–O stretch. The 3000 and 1500 cm^{-1} regions which are attributed to C–H stretching and bending, respectively, from the organic portion of the organoclays. The characteristic peaks of alkylammonium can occur at 2926 and 2852 cm^{-1} and are assigned to asymmetric stretch vibration of $-\text{CH}_3$ and $-\text{CH}_2$, respectively. The band at 1470 cm^{-1} is attributed to the

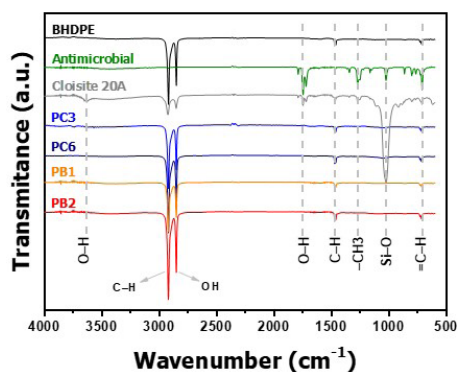


Figure 2. Infrared spectra of the BHDPE, Cloisite 20A® clay, antimicrobial agent, PB1, PB2, PC3, and PC6 systems.

symmetrical stretching vibration of $-\text{CH}_2$. Similar results for Cloisite 20A clay were reported by Naderi-Samani et al.^[41]. According to Pittol et al.^[42], the pirithione structure is shown in the band at 763 cm^{-1} , attributed to aromatic $=\text{C}-\text{H}$ out-of-plane deformation vibrations.

3.3 Thermal stability

TGA/DTG thermograms of BHDPE and their films containing clay (PC3 and PC6) and antimicrobial additives (PB1 and PB2) are in Figure 3. Nanocomposite films exhibited thermal stability similar to the control film (pure BHDPE) (Figure 3a). The degradation initiation temperature (T_{10}), referring to a 10% mass loss, the 50% mass loss (T_{50}), the peak temperature decomposition (T_p) (DTG peak in Figure 3b) and the percentage of residue at 550°C (R%) are reported in Table 2.

The T_{10} of BHDPE starts around 400°C^[25,43], and there was no variation for PB1, PB2, PC3, and PC6 systems, as shown in Figure 3 and Table 2. The clay and antimicrobial additive did not affect the film degradation temperatures (T_{10} and T_{50}). Similar results were found in nanocomposites of LDPE/EVA/graphene oxide^[43].

From T_p values, it was verified that PC3 and PC6 presented a reduction of approximately 7°C, PB2 of 3°C, and PB1 maintained this temperature compared with BHDPE film. Thus, the clay decreased the degradation temperature, while the antimicrobial additive did not compromise the thermal stability, according to the percentage of residue at 550°C (Table 2). The residue values at 550°C were consistent with previously reported works using LDPE/EVA^[25,42] and HDPE/clay^[21,23].

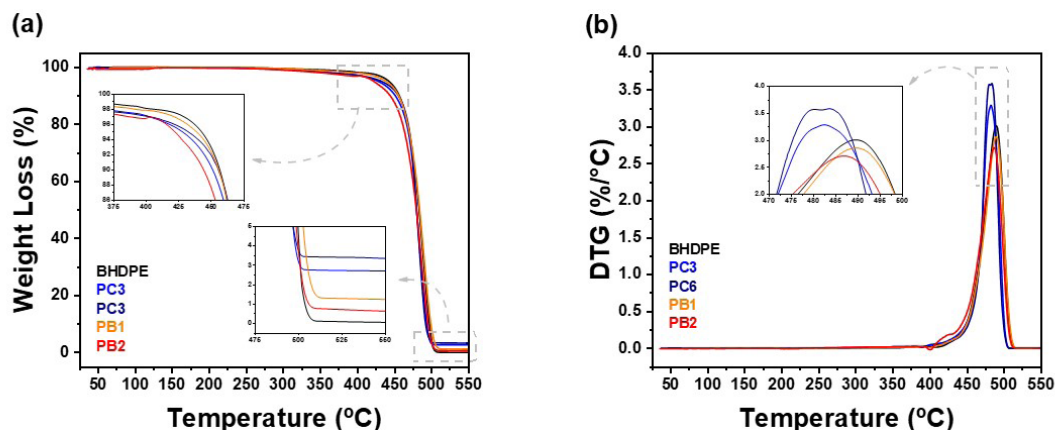


Figure 3. (a) TGA and (b) DTG of BHDPE, PB1, PB2, PC3, and PC6 systems.

Table 2. Thermal decomposition of the BHDPE, PB1, PB2, PC3, and PC6 systems and its residue.

Samples	T_{10} (°C)	T_{50} (°C)	T_p (°C)	R% (at 550°C)
BHDPE	456.6	483.2	489.4	0.08
PC3	451.1	479.8	482.3	2.70
PC6	455.5	479.9	483.4	3.34
PB1	455.8	484.1	489.5	1.25
PB2	454.3	479.6	486.7	1.89

3.4 Thermal behavior

Changes in the thermal transitions is verified through the results obtained by the DSC analyses. The thermal properties obtained: a melting temperature (T_m), heat of fusion (ΔH_m), and degree of crystallinity (X_c) are in Table 3.

The essential parameters for studying thermal properties were T_m and X_c . BHDPE had a T_m around 130°C ^[25,44,45]. Compositions with clay reduced of approximately 5°C for PC3 and 18°C for PC6 relative to BHDPE. Previous studies with HDPE and incorporation of 5 and 10 wt% of montmorillonite clay^[44] indicated a reduction in thermal stability for samples with 5 wt% of clay and an improvement in strength for those with 10 wt% of clay. Films with antimicrobial additives (PB1 and PB2) also reduced 12°C , possibly due to the EVA matrix responsible for carrying the antimicrobial agent.

As shown in Table 3, the evaluated X_c was lower about BHDPE, to a lesser extent for films with clay and films with antimicrobial additives. This behavior suggests that the EVA that supports the antimicrobial agent acted in the plasticization of polyethylene. Previous studies with LDPE/EVA/graphene oxide nanocomposites^[44] noted a decrease in T_m and X_c in systems containing only PE and EVA due to the partial miscibility of these two polymers.

3.5 Mechanical behavior

BHDPE films and their systems with additions of clay (PC3 and PC6) and antimicrobial additive (PB1 and PB2) were analyzed in uniaxial tensile tests, whose stress-strain curves are represented in Figure 4, and the mechanical properties (yield stress, tensile strength, strain at break, elastic modulus) are present in Table 4.

Generally, the predominance of ductile behavior can be observed where the material presents elastic behavior at

low deformations. After a specific stress, the film plastically deforms up to the rupture stress^[45]. The BHDPE films obtained a tensile strength of 58.8 ± 7.6 MPa, while the PC3 and PC6 films showed a reduction of 34.3% and an increase of 41.5%, respectively. The decrease in resistance for PC3 indicated the formation of agglomerates in the polymeric matrix, suggesting a microcomposite structure. The clay particle agglomerates acted as defects, altering the mechanical behavior^[8]. This behavior has been reported in several previous studies with bamboo fiber and particulate coconut shell hybrid PVC composite^[46] and polysulfone/ZnO composites^[47]. Also, comparing the behavior of the PC3 film with the BHDPE, there is a minor deformation with an increase in the modulus of elasticity^[48].

However, for PC6 films, an increase in tensile strength, deformation, and modulus of elasticity was observed, indicating that the clay in this composition was better dispersed^[49], corroborating the formation of a nanocomposite (Figure 1-b).

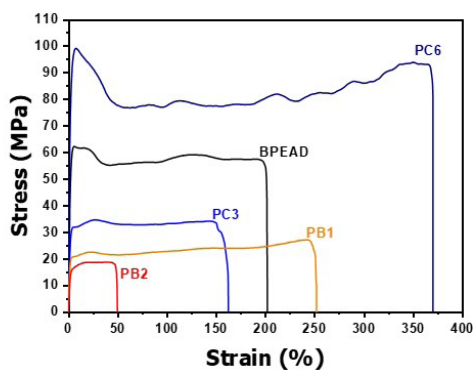


Figure 4. Representative stress-strain curves of BHDPE, PC3, PC6, PB1, and PB2 films.

Table 3. Thermal properties of BHDPE, PC3, PC6, PB1, and PB2 systems.

Samples	T_m ($^\circ\text{C}$)	ΔH_m ($\text{J}\cdot\text{g}^{-1}$)	X_c (%)
BHDPE	139.2	134.7	46.0
PC3	134.1	115.6	39.5
PC6	121.3	119.4	40.8
PB1	127.4	96.4	32.9
PB2	127.2	95.8	32.7

Table 4. Mechanical properties of BHDPE, PB1, PB2, PC3, and PC6 systems.

Material	Yield Stress (MPa)	Tensile Strength (MPa)	Strain at Break (%)	Elastic Modulus (MPa)
BHDPE	58.2 ± 7.1^b	58.8 ± 7.6^b	291.4 ± 11.1^b	1384.8 ± 38.6^c
PC3	33.1 ± 0.8^c	38.6 ± 4.7^c	231.7 ± 10.7^c	2692.2 ± 25.9^b
PC6	91.5 ± 12.9^a	83.2 ± 12.9^a	335.1 ± 12.9^a	5794.0 ± 82.1^a
PB1	25.7 ± 1.4^c	29.3 ± 1.1^{cd}	253.0 ± 4.8^c	1366.2 ± 56.3^c
PB2	15.3 ± 2.0^c	18.2 ± 2.0^d	50.7 ± 6.4^d	517.7 ± 38.0^d

Different letters (a-d) indicate a significant difference between the treatments by Tukey's test ($p < 0.05$).

The mechanical properties are influenced by the aspect ratio of charge, degree of charge dispersion in the polymeric matrix, and charge adhesion at the matrix interface. Antagonistic results due to the increase in clay content have already been reported^[26] as in aluminum oxide (Al_2O_3) nanoparticles^[49].

The antimicrobial additive affected the tensile strength. This property was reduced by almost 50% and 70% for PB1 and PB3 films, respectively. However, the lowest content of the microbial agent (PB1) did not significantly affect ($p < 0.05$) the modulus of concerning the pure BHDPE film. Nevertheless, the PB2 films showed a drastically reduced elastic modulus value, a recorded reduction of 62.9%. This behavior is related to the presence of EVA, the masterbatch matrix that contains the antimicrobial additive. The increase in EVA content implies a reduction in crystallinity^[50], as already reported by the DSC analyses (Table 3), and, consequently, may have promoted an increase in the mobility of the amorphous phases which causes a decrease in rigidity. Similar results were reported in previous studies due to the presence of EVA in PE/EVA/ZnO nanocomposites^[6] and in the HDPE/EVA blend^[50].

3.6 Antimicrobial activity

The antimicrobial activity behavior of BHDPE and its systems containing Cloisite 20A® and antimicrobial additives using the method of diffusion in liquid medium by *Staphylococcus aureus* bacteria is shown in Figure 5. Values for colony forming units ranged from 0.72 to 0.78 $\text{CFU}\cdot\text{mL}^{-1}$ and did not show significant difference ($p > 0.05$). Indicating that the presence of clay and commercial antimicrobial agent behaved similarly to pure polymer. Skoura et al.^[13] found no significant difference in antimicrobial activity against *S. aureus* when comparing the poly(caprolactone) matrix with intercalated nanocomposites filled with saponite clay organophilically modified using dimethyldioctadecylammonium bromide.

Organically modified clays can present antimicrobial activity due to the quaternary ammonium compounds that act in the adsorption of the microbial cell surface, diffusion, and disruption of the cytoplasmic membrane, causing cell death^[12,21,22]. The antimicrobial action of

quaternary ammonium compounds depends on their chemical structure, and the more hydrophobic ones, such as those present in Cloisite 20A®, may not impact microbial communities due to their low availability in the aqueous phase^[8]. On the other hand, the selected commercial antimicrobial agent, Sanitized® MB E 22-70, disrupts the cellular metabolic process of unwanted microorganisms like bacteria and fungi^[24].

The results corroborate that the amount of colony-forming units for PC3, PC6, PB1, and PB2 were close to that of BHDPE, which was the negative control. Studies with 2-vinyl pyridine-styrene-divinylbenzene copolymers in contact with the bacteria *Escherichia coli* did not show bactericidal activity for any of the evaluated concentrations^[50]. Similar behavior was reported in the study with reduced graphene oxide composites prepared by poly(3-(3'-thienyloxy)-propyltrimethyl-ammonium bromide) grafting^[51].

The antibacterial capacity of polymers depends not only on the efficiency of the introduced bactericidal group but also on the content of these groups and their accessibility by the contaminated solution^[21,22]. For packaging applications that require this antimicrobial control, it is necessary to develop polymeric supports with a physical-chemical structure that favors migration to the film surface and consequent diffusion in the medium.

The intercalated/exfoliated structure is characterized by the interaction between the barrier effect of clay particles and the catalytic effect of residual surfactant salts, which possibly impacted the predicted antimicrobial efficacy of organophilic clays^[52].

4. Conclusions

In this work, BHDPE flat films and their films containing Cloisite 20A® organoclays (PC3 and PC6) and antimicrobial additive (zinc pyrithione dispersed in EVA) (PB1 and PB2) were developed and evaluated. The addition of the antimicrobial additive did not promote changes in the crystalline structure of BHDPE. However, the addition of clay promoted displacement of the refraction peaks with increased in the basal interplanar distance, suggesting the formation of an intercalated/exfoliated nanocomposite. By FTIR spectra, it was noted the presence of clay into nanocomposites. However, it was impossible to differentiate the characteristic bands of EVA since there may have been overlapping of the bands or because of the low content in the composition. The degradation temperature did not change for PB1, but there was a 3°C reduction for the other films compared to pure BHDPE. A melting temperature and crystallinity were reduced in all systems. Both additives significantly affect ($p < 0,05$) all mechanical properties, with better results for films with 6 wt% of clay (PC6), and the different content of additives did not significantly reduce ($p > 0.05$) the proliferation of *Staphylococcus aureus* bacteria. Finally, it believes that flat films with promising properties were developed for application in packages that do not require biological control.

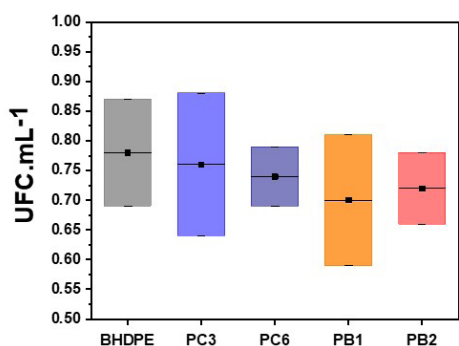


Figure 5. Counting of seed colony forming units of *Staphylococcus aureus*. The means are not significantly different ($p > 0.05$).

5. Author's Contribution

- **Conceptualization** – Renata Barbosa; Tatianny Soares Alves.
- **Data curation** – Priscylla Jordânia Pereira de Mesquita.
- **Formal analysis** – Priscylla Jordânia Pereira de Mesquita.
- **Funding acquisition** – Renata Barbosa.
- **Investigation** – Renata Barbosa; Tatianny Soares Alves; Priscylla Jordânia Pereira de Mesquita.
- **Methodology** – Priscylla Jordânia Pereira de Mesquita.
- **Project administration** – Renata Barbosa.
- **Resources** – Renata Barbosa; Tatianny Soares Alves.
- **Software** – Priscylla Jordânia Pereira de Mesquita; Cristiano José de Farias Braz.
- **Supervision** – Renata Barbosa; Tatianny Soares Alves.
- **Validation** – NA.
- **Visualization** – NA.
- **Writing – original draft** – Priscylla Jordânia Pereira de Mesquita; Cristiano José de Farias Braz.
- **Writing – review & editing** – Renata Barbosa; Tatianny Soares Alves.

6. Acknowledgements

The authors extend their appreciation to Universidade Federal do Piauí, Fundação de Amparo à Pesquisa do Estado do Piauí, and Conselho Nacional de Desenvolvimento Científico e Tecnológico (CNPq) for their valuable support. This research has been financially supported by CNPq [process number: 308446/2018-6] and [process number: 308309/2022-7].

7. References

1. Sima, V., Gheorghe, I. G., Subić, J., & Nancu, D. (2020). Influences of the Industry 4.0 revolution on the human capital development and consumer behavior: a systematic review. *Sustainability (Basel)*, *12*(10), 4035. <http://dx.doi.org/10.3390/su12104035>.
2. Angelopoulou, P., Giaouris, E., & Gardikis, K. (2022). Applications and prospects of nanotechnology in food and cosmetics preservation. *Nanomaterials (Basel, Switzerland)*, *12*(7), 1196. <http://dx.doi.org/10.3390/nano12071196>. PMID:35407315.
3. Siracusa, V., & Blanco, I. (2020). Bio-Polyethylene (Bio-PE), Bio-Polypropylene (Bio-PP) and Bio-Poly(ethylene terephthalate) (Bio-PET): recent developments in bio-based polymers analogous to petroleum-derived ones for packaging and engineering applications. *Polymers*, *12*(8), 1641. <http://dx.doi.org/10.3390/polym12081641>. PMID:32718011.
4. Porta, R., Sabbah, M., & Di Pierro, P. (2020). Biopolymers as food packaging materials. *International Journal of Molecular Sciences*, *21*(14), 4942. <http://dx.doi.org/10.3390/ijms21144942>. PMID:32668678.
5. Vilas, C., Mauricio-Iglesias, M., & García, M. R. (2020). Model-based design of smart active packaging systems with antimicrobial activity. *Food Packaging and Shelf Life*, *24*, 100446. <http://dx.doi.org/10.1016/j.fpsl.2019.100446>.
6. Galli, R., Hall, M. C., Breitenbach, E. R., Colpani, G. L., Zanetti, M., Mello, J. M. M., Silva, L. L., & Fiori, M. A. (2020). Antibacterial polyethylene - Ethylene vinyl acetate polymeric blend by incorporation of zinc oxide nanoparticles. *Polymer Testing*, *89*, 106554. <http://dx.doi.org/10.1016/j.polymeresting.2020.106554>.
7. Echeverria, C. A., Ozkan, J., Pahlevani, F., Willcox, M., & Sahajwalla, V. (2020). Multifunctional marine bio-additive with synergistic effect for non-toxic flame-retardancy and anti-microbial performance. *Sustainable Materials and Technologies*, *25*, e00199. <http://dx.doi.org/10.1016/j.susmat.2020.e00199>.
8. Li, Z., Wang, S., Yang, X., Liu, H., Shan, Y., Xu, X., Shang, S., & Song, Z. (2020). Antimicrobial and antifouling coating constructed using rosin acid-based quaternary ammonium salt and N-vinylpyrrolidone via RAFT polymerization. *Applied Surface Science*, *530*, 147193. <http://dx.doi.org/10.1016/j.apsusc.2020.147193>.
9. Scaffaro, R., Lopresti, F., Marino, A., & Nostro, A. (2018). Antimicrobial additives for poly(lactic acid) materials and their applications: current state and perspectives. *Applied Microbiology and Biotechnology*, *102*(18), 7739-7756. <http://dx.doi.org/10.1007/s00253-018-9220-1>. PMID:30009322.
10. Furko, M., Balázi, K., & Balázi, C. (2023). Calcium phosphate loaded biopolymer composites - a comprehensive review on the most recent progress and promising trends. *Coatings*, *13*(2), 360. <http://dx.doi.org/10.3390/coatings13020360>.
11. Dehghani, S., Peighambari, S. H., Peighambari, S. J., Hosseini, S. V., & Regenstein, J. M. (2019). Improved mechanical and antibacterial properties of active LDPE films prepared with combination of Ag, ZnO and CuO nanoparticles. *Food Packaging and Shelf Life*, *22*, 100391. <http://dx.doi.org/10.1016/j.fpsl.2019.100391>.
12. Bujdaková, H., Bujdaková, V., Májeková-Koščová, H., Gaálová, B., Bizovská, V., Boháč, P., & Bujdák, J. (2018). Antimicrobial activity of organoclays based on quaternary alkylammonium and alkylphosphonium surfactants and montmorillonite. *Applied Clay Science*, *158*, 21-28. <http://dx.doi.org/10.1016/j.clay.2018.03.010>.
13. Skoura, E., Boháč, P., Barlog, M., Pálková, H., Mautner, A., Bugyna, L., Bujdaková, H., & Bujdák, J. (2023). Structure, photoactivity, and antimicrobial properties of phloxine B / poly(caprolactone) nanocomposite thin films. *Applied Clay Science*, *242*, 107037. <http://dx.doi.org/10.1016/j.clay.2023.107037>.
14. Nasrollahzadeh, M., Shafiei, N., Baran, T., Pakzad, K., Tahsili, M. R., Baran, N. Y., & Shokouhimehr, M. (2021). Facile synthesis of Pd nanoparticles supported on a novel Schiff base modified chitosan-kaolin: antibacterial and catalytic activities in Sonogashira coupling reaction. *Journal of Organometallic Chemistry*, *945*, 121849. <http://dx.doi.org/10.1016/j.jorganchem.2021.121849>.
15. Nozha, S. G., Morgan, S. M., Ahmed, S. E. A., El-Mogazy, M. A., Diab, M. A., El-Sonbati, A. Z., & Abou-Dobara, M. I. (2021). Polymer complexes. LXXIV. Synthesis, characterization and antimicrobial activity studies of polymer complexes of some transition metals with bis-bidentate Schiff base. *Journal of Molecular Structure*, *1227*, 129525. <http://dx.doi.org/10.1016/j.molstruc.2020.129525>.
16. Li, W., Chen, M., Li, Y., Sun, J., Liu, Y., & Guo, H. (2020). Improving mildew resistance of soy meal by nano-Ag/TiO₂, Zinc Pyrrithione and 4-Cumylphenol. *Polymers*, *12*(1), 169. <http://dx.doi.org/10.3390/polym12010169>. PMID:31936509.

17. Official Journal of the European Union. (2021). *Commission Regulation (EU) 2021/1902 of 29 October 2021. Annexes II, III and V to Regulation (EC) No 1223/2009 of the European Parliament and of the Council as regards the use in cosmetic products of certain substances classified as carcinogenic, mutagenic or toxic for reproduction*. Retrieved in 2023, November 13, from <https://eur-lex.europa.eu/legal-content/EN/TXT/PDF/?uri=CELEX:32021R1902&from=EN>
18. Food and Drug Administration – FDA. (2023). *Inventory of Effective Food Contact Substance (FCS) Notifications*. Retrieved in 2023, November 13, from https://www.cfsanappsexternal.fda.gov/scripts/fdcc/index.cfm?set=FCN&id=2139&sort=FCN_No&order=DESC&startrow=1&type=basic&search=Pyrrithione
19. Marcous, A., Rasouli, S., & Ardestani, F. (2017). Low-density polyethylene films loaded by titanium dioxide and zinc oxide nanoparticles as a new active packaging system against *Escherichia coli* O157:H7 in fresh calf minced meat. *Packaging Technology & Science*, 30(11), 693-701. <http://dx.doi.org/10.1002/pts.2312>.
20. Rokbani, H., Daigle, F., & Ajji, A. (2019). Long- and short-term antibacterial properties of low-density polyethylene-based films coated with zinc oxide nanoparticles for potential use in food packaging. *Journal of Plastic Film & Sheeting*, 35(2), 117-134. <http://dx.doi.org/10.1177/8756087918822677>.
21. Hong, S.-I., Wang, L.-F., & Rhim, J.-W. (2022). Preparation and characterization of nanoclays-incorporated polyethylene/thermoplastic starch composite films with antimicrobial activity. *Food Packaging and Shelf Life*, 31, 100784. <http://dx.doi.org/10.1016/j.fpsl.2021.100784>.
22. Fasihnia, S. H., Peighambaroust, S. H., & Peighambaroust, S. J. (2018). Nanocomposite films containing organoclay nanoparticles as an antimicrobial (active) packaging for potential food application. *Journal of Food Processing and Preservation*, 42(2), e13488. <http://dx.doi.org/10.1111/jfpp.13488>.
23. Peighambaroust, S. H., Beigmohammadi, F., & Peighambaroust, S. J. (2016). Application of organoclay nanoparticle in low-density polyethylene films for packaging of UF cheese. *Packaging Technology & Science*, 29(7), 355-363. <http://dx.doi.org/10.1002/pts.2212>.
24. Sanitized®. (2013, May 24). *MB PE 23-70 Protects thermoplastic polymers against*. Burgdorf, Switzerland: Sanitized®.
25. Mesquita, P. J. P., Alves, T. S., & Barbosa, R. (2022). Development and characterization of green polyethylene/clay/antimicrobial additive nanocomposites. *Polímeros*, 32(2), e2022022. <http://dx.doi.org/10.1590/0104-1428.20210097>.
26. Tarani, E., Arvanitidis, I., Christofilos, D., Bikiaris, D. N., Chrissafis, K., & Vourlias, G. (2023). Calculation of the degree of crystallinity of HDPE/GNPs nanocomposites by using various experimental techniques: a comparative study. *Journal of Materials Science*, 58(4), 1621-1639. <http://dx.doi.org/10.1007/s10853-022-08125-4>.
27. Wunderlich, B., & Czornyj, G. (1977). A study of equilibrium melting of polyethylene. *Macromolecules*, 10(5), 906-913. <http://dx.doi.org/10.1021/ma60059a006>.
28. Nurazzi, N. M., Asyraf, M. R. M., Rayung, M., Norrahim, M. N. F., Shazleen, S. S., Rani, M. S. A., Shafi, A. R., Aisyah, H. A., Radzi, M. H. M., Sabaruddin, F. A., Ilyas, R. A., Zainudin, E. S., & Abdan, K. (2021). Thermogravimetric analysis properties of cellulosic natural fiber polymer composites: a review on influence of chemical treatments. *Polymers*, 13(16), 2710. <http://dx.doi.org/10.3390/polym13162710>. PMID:34451248.
29. American Society for Testing and Materials – ASTM. (2018). *ASTM D-882: Standard Test Method for Tensile Properties of Thin Plastic Sheeting*. Philadelphia, USA: ASTM International. Retrieved in 2023, November 13, from <https://www.astm.org/d0882-18.html>
30. Clinical and Laboratory Standards Institute – CSLI. (2023). *M100: Performance Standards for Antimicrobial Susceptibility Testing*. Malvern, Pennsylvania, USA: CSLI. Retrieved in 2023, November 13, from <https://clsi.org/about/press-releases/clsi-publishes-m100-performance-standards-for-antimicrobial-susceptibility-testing-33rd-edition/>
31. Clinical and Laboratory Standards Institute – CSLI. (2018). *M07: Methods for Dilution Antimicrobial Susceptibility Tests for Bacteria That Grow Aerobically*. Malvern, Pennsylvania, USA: CSLI. Retrieved in 2023, November 13, from https://clsi.org/media/1928/m07ed11_sample.pdf
32. Paiva, L. B., Morales, A. R., & Diaz, F. R. V. (2008). Organoclays: properties, preparation and applications. *Applied Clay Science*, 42(1-2), 8-24. <http://dx.doi.org/10.1016/j.clay.2008.02.006>.
33. Dias, G., Prado, M., Ligabue, R., Poirier, M., Le Roux, C., Micoud, P., Martin, F., & Einloft, S. (2018). Hybrid PU/synthetic talc/organic clay ternary nanocomposites: thermal, mechanical and morphological properties. *Polymers & Polymer Composites*, 26(2), 127-140. <http://dx.doi.org/10.1177/096739111802600201>.
34. Roy, A., Joshi, M., & Butola, B. S. (2019). Antimicrobial performance of polyethylene nanocomposite monofilaments reinforced with metal nanoparticles decorated montmorillonite. *Colloids and Surfaces. B, Biointerfaces*, 178, 87-93. <http://dx.doi.org/10.1016/j.colsurfb.2019.02.045>. PMID:30844564.
35. Jung, M. R., Horgen, F. D., Orski, S. V., & Rodriguez, C. (2018). Validation of ATR FT-IR to identify polymers of plastic marine debris, including those ingested by marine organisms. *Marine Pollution Bulletin*, 127, 704-716. <http://dx.doi.org/10.1016/j.marpolbul.2017.12.061>. PMID:29475714.
36. Stark, N. M., & Matuana, L. M. (2004). Surface chemistry changes of weathered HDPE/wood-flour composites studied by XPS and FTIR spectroscopy. *Polymer Degradation & Stability*, 86(1), 1-9. <http://dx.doi.org/10.1016/j.polydegradstab.2003.11.002>.
37. Terui, Y., & Hirokawa, K. (1994). Fourier transform infrared emission spectra of poly(vinyl acetate) enhanced by the island structure of gold. *Vibrational Spectroscopy*, 6(3), 309-314. [http://dx.doi.org/10.1016/0924-2031\(93\)E0065-A](http://dx.doi.org/10.1016/0924-2031(93)E0065-A).
38. Zhao, C., Qin, H., Gong, F., Feng, M., Zhang, S., & Yang, M. (2005). Mechanical, thermal and flammability properties of polyethylene/clay nanocomposites. *Polymer Degradation & Stability*, 87(1), 183-189. <http://dx.doi.org/10.1016/j.polydegradstab.2004.08.005>.
39. Cervantes-Uc, J. M., Cauich-Rodríguez, J. V., Vázquez-Torres, H., Garfias-Mesias, L. F., & Paul, D. R. (2007). Thermal degradation of commercially available organoclays studied by TGA-FTIR. *Thermochimica Acta*, 457(1), 92-102. <http://dx.doi.org/10.1016/j.tca.2007.03.008>.
40. Zhang, J., Gupta, R. K., & Wilkie, C. A. (2006). Controlled silylation of montmorillonite and its polyethylene nanocomposites. *Polymer*, 47(13), 4537-4543. <http://dx.doi.org/10.1016/j.polymer.2006.04.057>.
41. Naderi-Samani, H., Razavi, R. S., Loghman-Estarki, M. R., Ramazani, M., Barekat, M., Mishra, A. K., & Fattahi, H. (2019). The effects of Cloisite 20A content on the adhesion strength and corrosion behavior of poly (amide-imide)/cloisite 20A nanocomposite coatings. *Composites. Part B, Engineering*, 175, 107154. <http://dx.doi.org/10.1016/j.compositesb.2019.107154>.
42. Pittol, M., Tomacheski, D., Simões, D. N., Ribeiro, V. F., & Santana, R. M. C. (2017). Antimicrobial performance of thermoplastic elastomers containing zinc pyrithione and silver nanoparticles. *Materials Research*, 20(5), 1266-1273. <http://dx.doi.org/10.1590/1980-5373-mr-2017-0137>.
43. Boronat, T., Fombuena, V., Garcia-Sanoguera, D., Sanchez-Nacher, L., & Balart, R. (2015). Development of a biocomposite based on green polyethylene biopolymer and eggshell. *Materials & Design*, 68, 177-185. <http://dx.doi.org/10.1016/j.matdes.2014.12.027>.

44. Pu, S., Hao, Y.-B., Dai, X.-X., Zhang, P.-P., Zeng, J.-B., & Wang, M. (2017). Morphological, rheological, crystalline and mechanical properties of ethylene-vinyl acetate copolymer/linear low-density polyethylene/amphiphilic graphene oxide nanocomposites. *Polymer Testing*, *63*, 289-297. <http://dx.doi.org/10.1016/j.polymertesting.2017.08.028>.
45. Vozniak, A., & Bartczak, Z. (2022). Plastic deformation of high density polyethylene with extended-chain crystal morphology. *Polymers*, *15*(1), 66. <http://dx.doi.org/10.3390/polym15010066>. PMID:36616416.
46. Adediran, A. A., Akinwande, A. A., Balogun, O. A., Olasoju, O. S., & Adesina, O. S. (2021). Experimental evaluation of bamboo fiber/particulate coconut shell hybrid PVC composite. *Scientific Reports*, *11*(1), 5465. <http://dx.doi.org/10.1038/s41598-021-85038-3>. PMID:33750871.
47. Dadashov, S., Demirel, E., & Suvaci, E. (2022). Tailoring microstructure of polysulfone membranes via novel hexagonal ZnO particles to achieve improved filtration performance. *Journal of Membrane Science*, *651*, 120462. <http://dx.doi.org/10.1016/j.memsci.2022.120462>.
48. Santos, M. S., Montagna, L. S., Rezende, M. C., & Passador, F. R. (2019). A new use for glassy carbon: development of LDPE/glassy carbon composites for antistatic packaging applications. *Journal of Applied Polymer Science*, *136*(11), 47204. <http://dx.doi.org/10.1002/app.47204>.
49. Sonia, P., Jain, J. K., Singhal, P., & Saxena, K. K. (2021). Performance evaluation of hybrid polymer nanocomposite. *Materials Today: Proceedings*, *44*(Part 1), 1659-1663. <http://dx.doi.org/10.1016/j.matpr.2020.11.826>.
50. Savini, G., & Oréfice, R. L. (2021). Super ductility in HDPE/EVA blends triggered by synthetic amorphous nanotalc. *Journal of Polymer Research*, *28*(1), 19. <http://dx.doi.org/10.1007/s10965-020-02389-7>.
51. Xiao, L., Sun, J., Liu, L., Hu, R., Lu, H., Cheng, C., Huang, Y., Wang, S., & Geng, J. (2017). Enhanced photothermal bactericidal activity of the reduced graphene oxide modified by cationic water-soluble conjugated polymer. *ACS Applied Materials & Interfaces*, *9*(6), 5382-5391. <http://dx.doi.org/10.1021/acsami.6b14473>. PMID:28112908.
52. Worasith, N., & Goodman, B. A. (2023). Clay mineral products for improving environmental quality. *Applied Clay Science*, *242*, 106980. <http://dx.doi.org/10.1016/j.clay.2023.106980>.

Received: Nov. 13, 2023

Revised: Feb. 11, 2024

Accepted: Feb. 23, 2024